Simultaneous interplanetary scintillation and Heliospheric Imager observations of a coronal mass ejection

G. D. Dorrian,[1] A. R. Breen,[1] D. S. Brown,[1] J. A. Davies,[2] R. A. Fallows,[1] and A. P. Rouillard[3]

Received 2 October 2008; revised 18 November 2008; accepted 24 November 2008; published 31 December 2008.

[1] We describe simultaneous Interplanetary Scintillation (IPS) and STEREO Heliospheric Imager (HI) observations of a coronal mass ejection (CME) on 16 May 2007. Strong CME signatures were present throughout the IPS observation. The IPS raypath lay within the field-of-view of HI-1 on STEREO-A and comparison of the observations shows that the IPS measurements came from a region within a faint CME front observed by HI-1A. This front may represent the merging of two converging CMEs. Plane-of-sky velocity estimates based on time-height plots of the two converging CME structures were 325 kms^{-1} and 550 kms^{-1} for the leading and trailing fronts respectively. The plane-of-sky velocities determined from IPS ranged from 420 ± 10 kms^{-1} to 520 ± 20 kms^{-1}. IPS results reveal the presence of micro-structure within the CME front which may represent interaction between the two separate CME events. This is the first time that it has been possible to interpret IPS observations of small-scale structure within an interplanetary CME in terms of the global structure of the event. **Citation:** Dorrian, G. D., A. R. Breen, D. S. Brown, J. A. Davies, R. A. Fallows, and A. P. Rouillard (2008), Simultaneous interplanetary scintillation and Heliospheric Imager observations of a coronal mass ejection, *Geophys. Res. Lett.*, *35*, L24104, doi:10.1029/2008GL036181.

1. Introduction

[2] Interplanetary scintillation (IPS) was first described by *Hewish et al.* [1964]. When the raypath from a compact radio source passes through the solar wind it encounters regions of varying plasma density, inducing phase variations. As the wave continues to the receiver these phase variations are converted into amplitude variations by interference [e.g., *Coles*, 1978].

[3] The sensitivity of this technique is heavily weighted towards scattering events that occur around the point of closest approach of the raypath to the Sun (the P-point). Solar wind density falls off approximately as $1/R^2$ (where R is the distance from the Sun) and as the production of phase scintillations by small-scale density variations in the solar wind is roughly proportional to the square of the local electron density, the amount of scattering produced falls off as $1/R^4$.

[4] If the radio source is observed with two antennas when the projection into the plane of the sky of the baseline between them is close to parallel to the outflow direction of the solar wind, then amplitude variation patterns received at the two antennas will be significantly correlated. The maximum cross-correlation occurs at a time-lag which depends on the velocity of the solar wind irregularities and the radial component of the plane-of-sky projection of the antenna separation [e.g., *Armstrong and Coles*, 1972; *Breen et al.*, 1996].

[5] More thorough investigation of the cross-correlation function can yield further solar wind properties, such as the spatial size of the irregularities, the velocities of multiple solar wind streams crossing the raypath, and reveal the presence of transient solar wind features. The presence of a CME in the raypath can be recognised by the appearance of some or all of the following signatures [*Canals*, 2002; *Jones et al.*, 2007]: (1) a rapid variation (on timescales of hours or less) of the solar wind speed; (2) a negative lobe in the cross-correlation function near zero time-lag, produced by a rotation of the interplanetary magnetic field in the raypath [*Klinglesmith*, 1997]; (3) a rapid variation (on timescales of hours or less) in the shape of the cross-correlation function; and (4) a rapid variation (increases/decreases) in scintillation signal strength on timescales of hours or less.

[6] These signatures correspond to those used for identifying CMEs in coronagraphic data [*Hundhausen et al.*, 1984] or from in-situ measurements of magnetic field direction.

[7] The Heliospheric Imager on the STEREO-A and B spacecraft consist of two white-light, wide-field refracting telescopic imagers, HI-1 and HI-2, which observe light scattered from the solar wind. The field-of-view of HI-1 on STEREO-A (HI-1A) is centred at 14° from Sun centre, has a 20° angular extent and is shielded from incident sunlight by a series of baffles [e.g., *Eyles et al.*, 2008]. Background scattered light from the F-corona incident on the imagers is removed by image processing procedures [e.g., *Harrison et al.*, 2005, *Eyles et al.*, 2008]. After background subtraction and calibration [e.g., *Brown et al.*, 2008], HI-1 is sensitive to solar wind structure luminosities exceeding 3×10^{-15} solar brightness. This is essential as scattered light from CME structure is frequently around 10^2 times fainter than the F-corona [e.g., *Harrison et al.*, 2005, 2007]. In this study the regions observed with IPS lay wholly within the field-of-view of HI-1A.

[8] Simultaneous IPS and HI observations of CMEs made when the IPS raypath intersects the HI field-of-view enable direct comparison of results. In white-light observations the

[1]Institute of Mathematics and Physics, Aberystwyth University, Aberystwyth, UK.
[2]Space Science and Technology Department, Rutherford Appleton Laboratory, Didcot, UK.
[3]Department of Physics and Astronomy, Southampton University, Southampton, UK.

0094-8276/08/2008GL036181$05.00

intensity of scattered light from a unit volume is proportional to the electron density, but the production of IPS is roughly proportional to the square of the electron density. HI thus provides an overall view of the CME, whilst the point measurement of IPS provides information on a small part of the structure.

[9] A complicating factor is the difference in the distance from the observer to the scattering location in the two techniques. In white-light imaging, the instruments detect solar photons scattered by the solar wind. Scattering events farther from the observer are harder to detect as there is a $1/d^2$ dependence for received intensity of scattered light, where d is the distance from the scattering event to the observer. In IPS the proportion of phase variation converted by interference to amplitude scintillation increases with path length from the scattering event and so is greater for scattering events further from the observer. Thus, for observations of solar wind structures at equal distances from the Sun, white light observations are more sensitive to those nearer Earth, while IPS sensitivity is lower for near-Earth structures [e.g., *Hewish*, 1989].

[10] The CME which will be described in this paper originated close to the solar limb, so in this particular case the discrepancies introduced by the different dependencies on observer distance are small, simplifying analysis. A more detailed description of how IPS and HI observations are combined will be given in an upcoming substantive paper.

2. Observations

2.1. Geometry

[11] Direct comparisons between data from HI and IPS are only possible if the same region of the CME is observed simultaneously by the two instruments. To determine whether the CME discussed in this paper and imaged by HI-1A produced the IPS CME signatures it is necessary to identify where in the HI-1A image the IPS P-point (P′) lay. This was established by calculating angle A, the Sun-spacecraft-P′ angle (see Figure 1), derived from the distances of the spacecraft to the Sun and of the IPS P-point to the Sun.

[12] On 16 May 2007, when IPS CME signatures were observed, the Sun to STEREO-A distance was 206.3 solar radii (R_S) and the Sun to P-point distance was $52.2R_S$ for observations of J0431 + 206, giving A = 13.40°.

[13] The calculation of P′ assumes that Earth and STEREO-A both lie in the ecliptic. This is not strictly true but the angular separation between the ecliptic, Earth, and STEREO-A was <1°. The difference in position of P and P′ at the time of these observations arises from the small difference in heliocentric longitude of Earth and STEREO-A (5.42°). P and P′ therefore lie close together and are assumed to observe the same region of the CME, so that it is likely that signatures seen in IPS come from the region of the CME passing over P′ at the time of the IPS observations.

2.2. HI-1A Observations

[14] HI-1A was observing in normal synoptic mode on 16 May 2007 when it detected a CME propagating from the East limb of the Sun. The structure was visible in the inner part of the field of view by 0730 UT. Figures 2a–2c are produced after a 3 day minimum intensity background was subtracted to remove light from the F-corona as discussed by *Eyles et al.* [2008]. The time-height plot shown in Figure 2d was composed from a series of such images. Closer investigation revealed the presence of a faint front ahead of the main structure (seen as features A and B in Figure 2d, and as the enhancement in HI-1A pixel intensity around 1100 UT in Figure 4e).

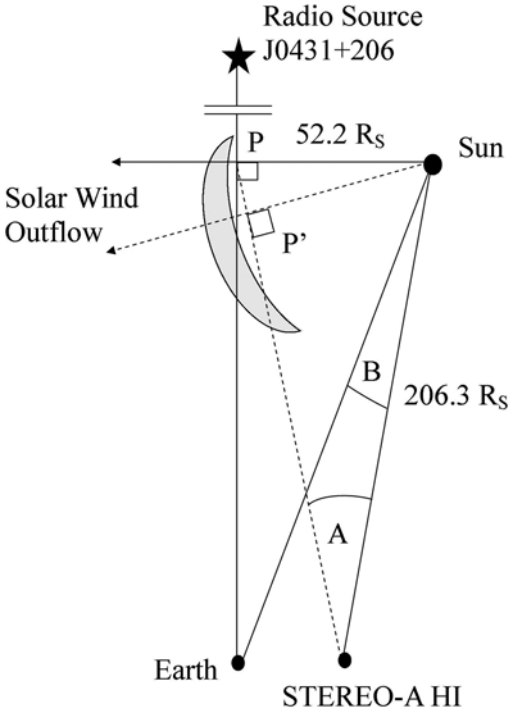

Figure 1. Schematic diagram of the geometry of the IPS raypath and the STEREO-A spacecraft on 16 May 2007 at 1330 UTC, as well as a (arbitrary) CME position indicated by the shaded crescent. Distances given are in R_S. The P-point is labelled P and the apparent position of the P-point in the HI-1A images is denoted as P′. P′ also indicates the location of closest approach to the Sun for HI-1A along that line-of-sight. Angle B was 5.42° at the time of the observations on the 16th, ensuring that the distance between P and P′ was very small compared to the size of the CME.

[15] The gradients of visible features in this time-height plot provide estimates of the average plane-of-sky velocities for each feature. Feature A has a plane-of-sky velocity of approximately 325 kms^{-1}. Feature B has a plane-of-sky velocity of about 550 kms^{-1}.

2.3. IPS Observations of the Background Solar Wind on 15 May 2007

[16] The EISCAT UHF system [*Rishbeth and Williams*, 1985; *Bourgois et al.*, 1985], comprises three antennas. The Kiruna and Sodankylä antennas receive at 1420 MHz, Tromsø at 928 MHz. Dual frequency IPS observations have been made at EISCAT since 2002 [*Fallows et al.*, 2006, 2008]. The P-point for radio source J0431 + 206 on 15 May 2007 lay at a heliocentric distance of $55.3R_S$ and a heliographic latitude of 11.8°S. Observations began at 1700 UT and lasted for 15 minutes. The plane-of-sky velocity derived from the time lag of peak correlation between the Tromsø and Sodankylä signals was 500 ± 55 kms^{-1}.

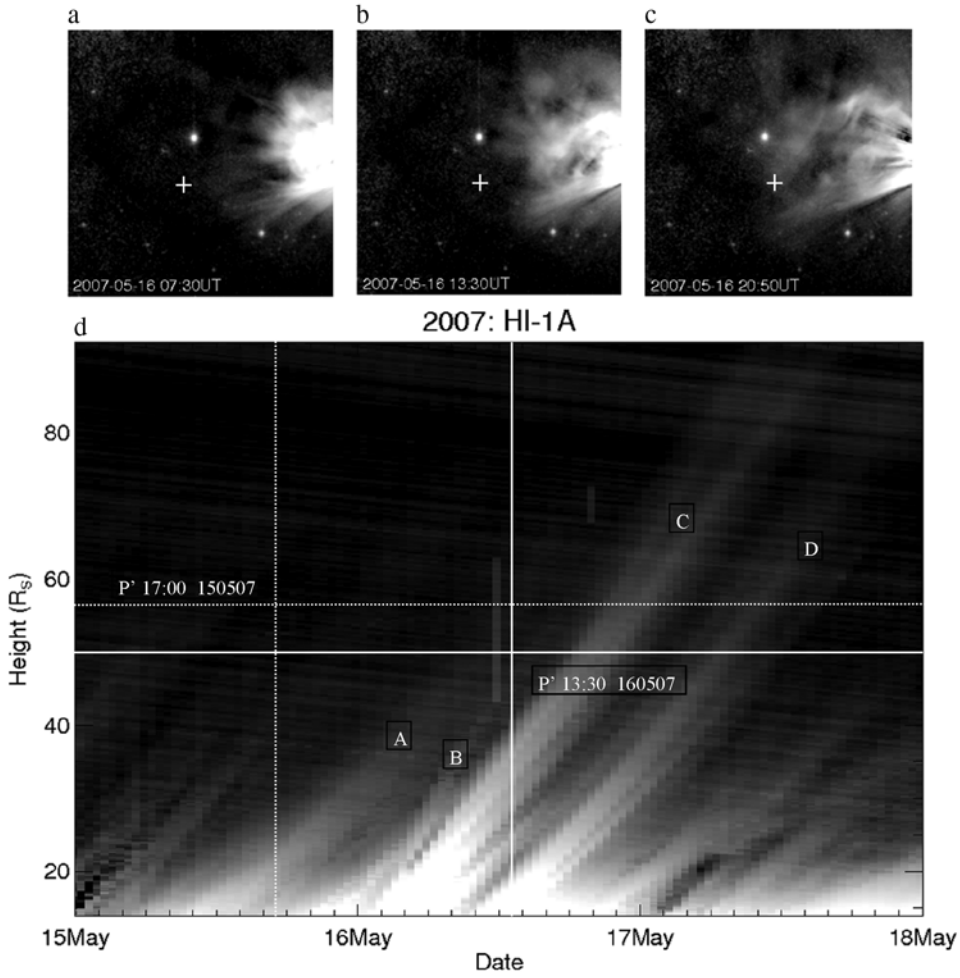

Figure 2. (a)–(c) Three day background-subtracted images obtained from HI-1A, showing the CME propagating into the heliosphere. Scattered light from the F-corona has been subtracted from these images. (d) A time-height plot for the time period in question with the position of P′ at the time of the IPS observations overlaid and labelled. The plane-of-sky velocity for features A and B are 325 kms^{-1} and 550 kms^{-1} respectively. The IPS observations on 16 May began at 1330 UT and the position of P′ is denoted by the white cross and yielded plane-of-sky velocities ranging from 420 kms^{-1} to 520 kms^{-1} over the observation period. At 1330 UT, P′ lies some distance ahead of the main structures of the CME (features C and D).

[17] The scintillation signal strength was low and as a result only a single estimate of velocity and 6 scintillation level estimates could be obtained. These measurements illustrate solar wind conditions prior to the onset of CME signatures seen on the following day (Figure 3a).

2.4. IPS Observations of a CME on 16 May 2007

[18] The same radio source was observed for 30 minutes on 16 May 2007, using Kiruna and Sodankylä. The P-point for observations of J0431 + 206 lay at a heliocentric distance of 52.2 R_S and a heliographic latitude of 12.1°S. Figure 3b shows the cross-correlation result obtained for the 1335-1340 UT time bin and is representative of results throughout the observation. A clear anti-correlation near the zero lag was present throughout these observations.

[19] Scintillation levels were also significantly greater, making more detailed investigation of the variability of the cross-correlation function possible. The data have been analysed in 10 minute time blocks, with each successive block advancing by 1 minute. Thus the first block covers 1330-1340 UT, the second covers 1331-1341 UT etc up to the last at 1350-1400 UT. The IPS observation times stated in Figure 4 and throughout this paper therefore indicate the first minute of each time block.

[20] Within each block, relative scintillation level and the plane-of-sky velocity corresponding to the peak in cross-correlation were calculated. The relative scintillation level is represented in this case by the area under the 0.15 Hz to 3 Hz segment of the power spectrum. This covers the scintillation part of the spectrum while excluding most of the low-frequency system variations and high frequency noise [*Fallows et al.*, 2002]. The pass band was kept constant for the duration of the observations. The plane-of-sky velocity estimates were obtained with power spectrum filter values set between 0.15 Hz and 5 Hz. The scintillation level for each antenna and the velocity data are displayed in Figure 4 for each start time of the 10 minute data blocks, together

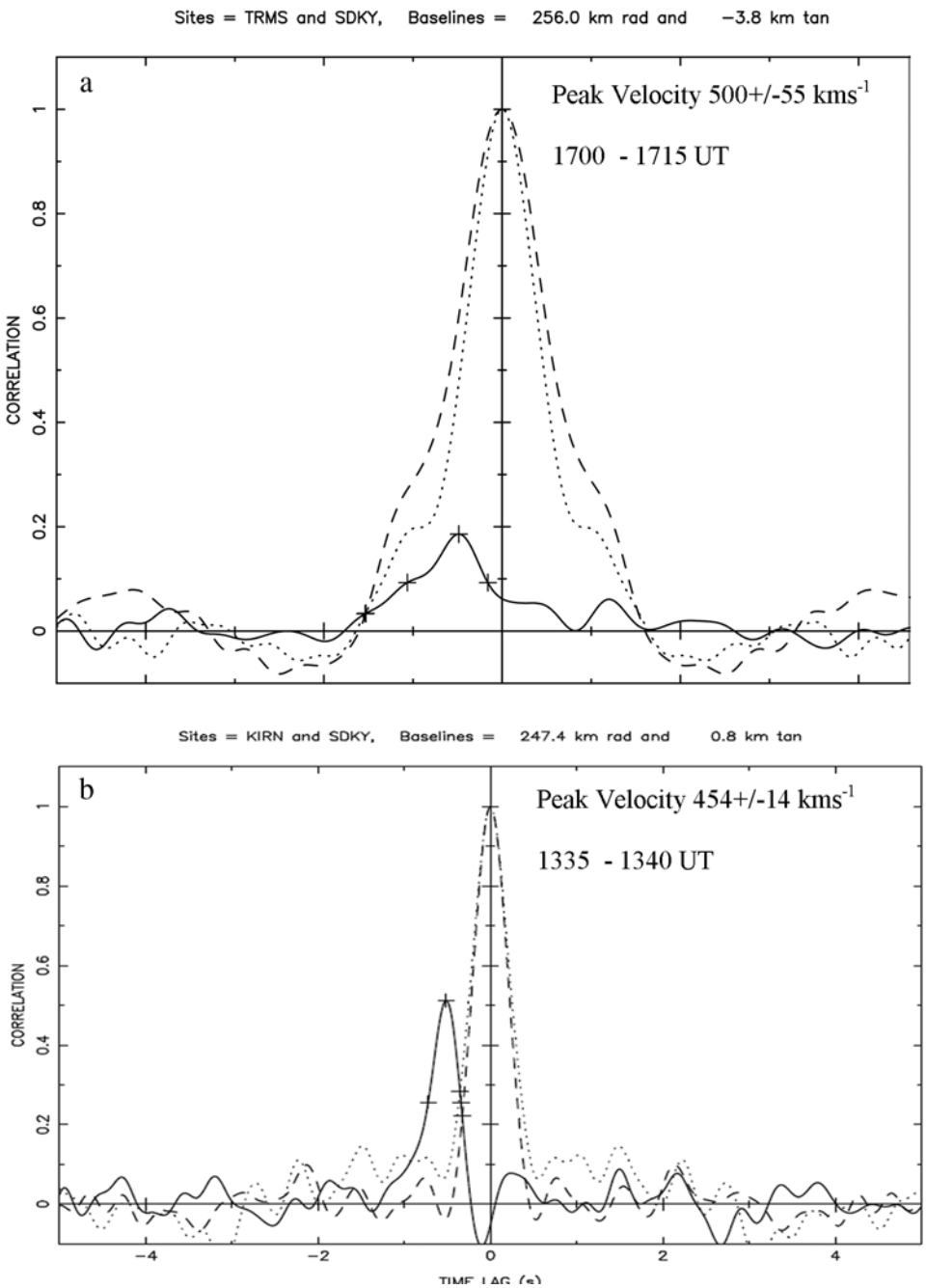

Figure 3. (a) Tromsø/Sodankylä cross-correlation function for the full 15 minutes of observation of J0431 + 206 on 15 May 2007. The dashed and dotted lines represent the auto-correlation function [e.g., *Coles*, 1978] for Tromsø and Sodankylä respectively and the solid line represents the cross-correlation function. (b) A sample cross-correlation function derived from 5 minutes of observations from Kiruna and Sodankylä of J0431 + 206 from 1335–1340 UT on 16 May, typical of results for the entire observation. Unlike the profile shown in Figure 3a, this exhibits a significant level of anti-correlation near zero lag, a significant increase in cross-correlation and a reduced uncertainty in the velocity estimate in spite of the reduced integration time – a result of the increased scintillation strength.

with the equivalent data from 15 May 2007. The units for scintillation levels are normalised and arbitrary.

3. Discussion

[21] IPS observations of J0431 + 206 on 15 and 16 May 2007 show considerably different correlation profiles and plane-of-sky solar wind speeds. A marked level of anti-correlation near zero time-lag appears in the cross-correlation functions from the 16 May 2007 observations. This was not present on the previous day, and together with the increase in scintillation level this strongly suggests the arrival of CME structure, including a significant rotation of the local interplanetary magnetic field, in the raypath between the

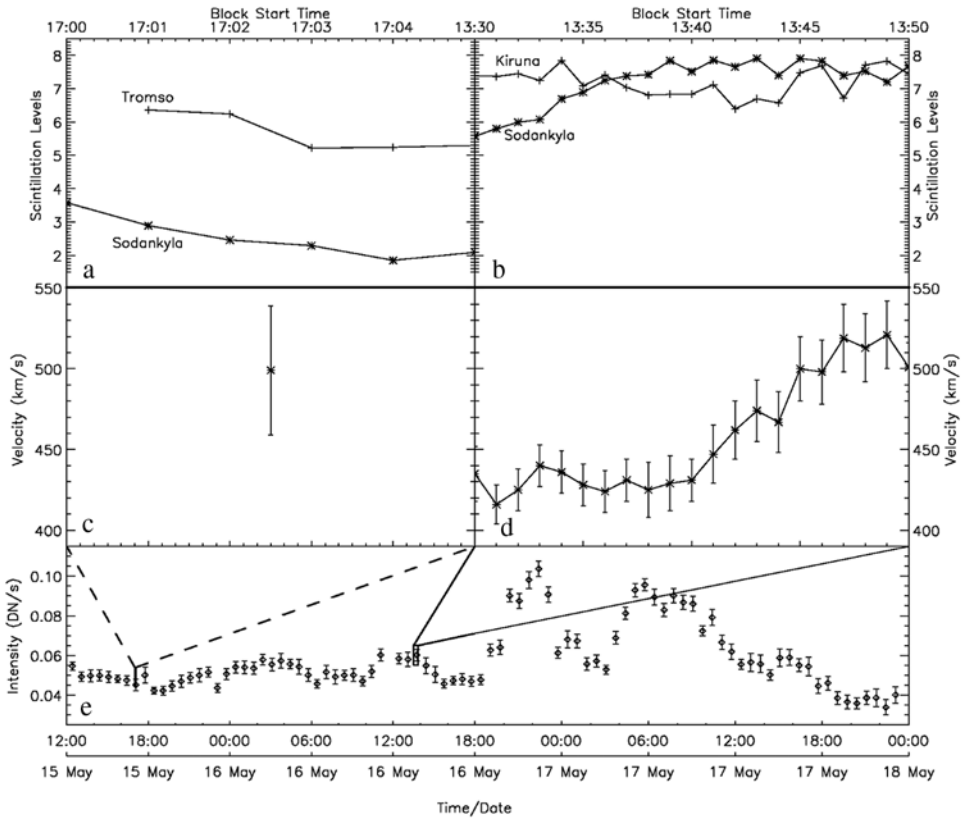

Figure 4. Scintillation levels recorded at (a) Tromsø/Sodankylä on 15 May 2007 (before the arrival of the CME in the raypath) and (b) Kiruna/Sodankylä on 16 May 2007 (during CME passage across the raypath). Scintillation level is expressed in arbitrary units. The first data point for Tromsø on 15 May 2007 is missing because the antenna was still moving to observe the radio source in the first minute; hence data for the first 10 minute block were partially recorded from an off-source position. Scintillation levels on 16 May 2007 are noticeably higher than those from 15 May. (c) and (d) Plane-of-sky velocity data, from the same observations. The single velocity data point obtained on 15 May is from cross-correlation of the Tromsø/Sodankylä antennas, whereas velocity data on 16 May is from the Kiruna/Sodankylä antennas. (e) The white-light intensity measured in the HI-1A pixel corresponding to P′. The IPS measurements on 16 May 2007 lie within the first faint front of the CME.

observations on 15 and 16 May. This is supported by the fact that the anti-correlation near zero time-lag is present at the start of the observations on 16 May 2007.

[22] Scintillation levels for 10 minute integration periods observed independently on two separated antennas both show increasingly variable behaviour (Figure 4b) beginning approximately at the 1340 UT time integration bin. This corresponds to a steady increase in plane-of-sky solar wind velocity (Figure 4d) which was 426 kms^{-1} at the start of the observing period. This had risen to a maximum of 523 kms^{-1} for the 10 minute integration beginning at 1349 UT. The sudden increase in plane-of-sky solar wind velocity (and the simultaneous increase in the variability of scintillation levels) demonstrates that significant changes in solar wind conditions can occur on timescales of minutes and reveals the presence of considerable small-scale structural variability.

[23] Comparison with HI-1A results (Figure 4) suggests that the first faint front of the CME structure reached P′ around 1100 UT on 16 May 2007. This is consistent with arrival times for features A and B (Figure 2d). This faint feature was followed by two large and distinct fronts which passed over P′ at about 1800 UT on 16 May 2007 and 0300 UT on 17 May 2007 – well after the end of the IPS observation. The IPS observations made between 1330 UT and 1400 UT therefore show structure within this first faint front. In contrast the HI-1A pixel intensity at P′ on 15 May 2007 was noticeably lower and less variable. This is consistent with the weaker scintillation levels and absence of CME signatures in the IPS cross-correlation profile from 15 May 2007.

[24] The plane-of-sky IPS velocities on 16 May 2007 were intermediate between those from HI-1A for features A (325 kms^{-1}) and B (550 kms^{-1}) shown in Figure 2, with an increase in IPS speeds seen from 1340 UT. The mean of the velocities of event A and B is comparable to the velocities obtained from IPS at the start of the observation (1330-1340 UT), with the highest IPS speeds (seen near the end of the observation) being close to the speed of feature B. The angular separation between Earth and STEREO-A was small and the plane-of-sky from each location would have been slightly different which may give rise to the small velocity discrepancies between both techniques. It should also be noted that the cadence of HI-1A (40 minutes) is considerably lower than the time resolution for the IPS data so that HI-1A velocity estimates represent averages across the large-scale structure of the front.

[25] Extreme ultra-violet observations from EUVI on STEREO-A and B show that both CME features A and B were launched from near the isolated active region 10956. The longitudinal extent of this active region was much less than the likely longitudinal angular extents of either CME (assuming the events were initially rotationally symmetrical [e.g., *Jones et al.*, 2007]) and solar rotation in the 12 hours between the events was insufficient to prevent their paths overlapping, we interpret the IPS results as showing interaction between feature A and the faster feature B. Complex structure revealed in the IPS measurements may be consistent with this interpretation.

[26] The geometry of the HI-1A field-of-view and the IPS raypath in this observation make the 16 May 2007 CME a particularly suitable case study for comparing the HI and IPS results. Combined IPS and white-light coronal CME observations have been made before [e.g., *Lynch et al.*, 2002] but this is the first time that IPS signatures of an interplanetary CME have been directly and unambiguously associated with a specific region seen in white-light images. The observations are of particular interest in that they reveal the small-scale structure present within CME fronts, and can potentially provide new information on interaction between CMEs.

[27] **Acknowledgments.** The authors would like to thank the directors and staff of EISCAT for their help and for the data used here. We thank W. A. Coles and B. J. Rickett for the use of their IPS analysis routines. HI was developed by a collaboration including RAL and the University of Birmingham (both UK), CSL (Belgium) and NRL (US). We acknowledge the support of STFC (UK).

References

Armstrong, J. W., and W. A. Coles (1972), Analysis of three-station interplanetary scintillation, *J. Geophys. Res.*, *77*, 4602–4610.

Bourgois, G., G. Daigne, W. Coles, J. Silen, T. Turunen, and P. Williams (1985), Measurements of the solar wind velocity with EISCAT, *Astron. Astrophys.*, *144*, 452–462.

Breen, A., W. Coles, R. Grall, U.-P. Løyhaug, J. Markkanen, H. Misawa, and P. Williams (1996), EISCAT measurements of interplanetary scintillation, *J. Atmos. Terr. Phys.*, *58*, 507–519.

Brown, D. S., D. Bewsher, and C. J. Eyles (2008), Calibrating the pointing and optical parameters of the STEREO Heliospheric Imagers, *Sol. Phys.*, in press.

Canals, A. (2002), Interplanetary scintillation studies of the solar wind during the rising phase of the solar cycle, Ph.D. thesis, Univ. of Wales, Aberystwyth, U. K.

Coles, W. (1978), Interplanetary scintillation, *Space Sci. Rev.*, *21*, 411–425.

Eyles, C. J., et al. (2008), The Heliospheric Imagers on-board the STEREO mission, *Sol. Phys.*, in press.

Fallows, R. A., P. Williams, and A. Breen (2002), EISCAT measurements of solar wind velocity and the associated level of interplanetary scintillation, *Ann. Geophys.*, *20*, 1279–1289.

Fallows, R. A., A. Breen, M. Bisi, R. Jones, and G. Wannberg (2006), Dual-frequency interplanetary scintillation observations of the solar wind, *Geophys. Res. Lett.*, *33*(11), L11106, doi:10.1029/2006GL025804.

Fallows, R. A., A. Breen, and G. Dorrian (2008), Developments in the use of EISCAT for interplanetary scintillation, *Ann. Geophys.*, *26*, 2229–2236.

Harrison, R. A., et al. (2005), The STEREO heliosphere imager: How to detect CMEs in the heliosphere, *Adv. Space Res.*, *36*, 1512–1523.

Harrison, R. A., et al. (2007), First imaging of coronal mass ejections in the heliosphere viewed from outside the Sun-Earth line, *Sol. Phys.*, *247*, 171–193.

Hewish, A. (1989), A user's guide to scintillation, *J. Atmos. Terr. Phys.*, *51*, 743–750.

Hewish, A., P. Scott, and D. Wills (1964), Interplanetary scintillation of small diameter radio sources, *Nature*, *203*, 1214–1217.

Hundhausen, A. J., C. B. Sawyer, L. House, R. M. E. Illing, and W. J. Wagner (1984), Coronal Mass ejections observed during the solar maximum mission: Latitude distribution and rate of occurrence, *J. Geophys. Res.*, *89*, 2639–2646.

Jones, R. A., A. Breen, R. Fallows, A. Canals, M. Bisi, and G. Lawrence (2007), Interaction between coronal mass ejections and the solar wind, *J. Geophys. Res.*, *112*, A08107, doi:10.1029/2006JA011875.

Klinglesmith, M. T. (1997), The polar solar wind from 2.5 to 40 solar radii: Results from intensity scintillation observations, Ph.D. thesis, Univ. of Calif., San Diego, La Jolla.

Lynch, B. J., W. A. Coles, and N. R. Sheeley Jr. (2002), A comparison of mean density and micro scale density fluctuations in a CME at $10R_S$, *Geophys. Res. Lett.*, *29*(19), 1913, doi:10.1029/2001GL014152.

Rishbeth, H., and P. Williams (1985), The EISCAT ionospheric radar: The system and its early results, *Q. J. R. Astron. Soc.*, *26*, 478–512.

A. R. Breen, D. S. Brown, G. D. Dorrian, and R. A. Fallows, Institute of Mathematics and Physics, Aberystwyth University, Aberystwyth SY23 2AX, UK. (gdd05@aber.ac.uk)

J. A. Davies, Space Science and Technology Department, Rutherford Appleton Laboratory, Didcot OX11 0QX, UK.

A. P. Rouillard, Deptartment of Physics and Astronomy, Southampton University, Southampton SO17 1BJ, UK.